RESEARCH ARTICLE

# Evaluation of articular cartilage with quantitative MRI in an equine model of post-traumatic osteoarthritis

Abdul Wahed Kajabi[1,2]  |  Victor Casula[1,2]  |  Jaakko K. Sarin[3,4]  |  Juuso H. Ketola[1]  |
Olli Nykänen[3]  |  Nikae C. R. te Moller[5]  |  Irina A. D. Mancini[5]  |  Jetze Visser[6]  |
Harold Brommer[5]  |  P. René van Weeren[5]  |  Jos Malda[5,6]  |  Juha Töyräs[3,4,7]  |
Miika T. Nieminen[1,2,8]  |  Mikko J. Nissi[1,3]

[1]Research Unit of Medical Imaging, Physics and Technology, University of Oulu, Oulu, Finland

[2]Medical Research Center Oulu, University of Oulu and Oulu University Hospital, Oulu, Finland

[3]Department of Applied Physics, University of Eastern Finland, Kuopio, Finland

[4]Diagnostic Imaging Center, Kuopio University Hospital, Kuopio, Finland

[5]Department of Clinical Sciences, Faculty of Veterinary Medicine, Utrecht University, Utrecht, the Netherlands

[6]Department of Orthopaedics, University Medical Center Utrecht, the Netherlands

[7]School of Information Technology and Electrical Engineering, The University of Queensland, Brisbane, Australia

[8]Department of Diagnostic Radiology, Oulu University Hospital, Oulu, Finland

**Correspondence**
Abdul Wahed Kajabi, Research Unit of Medical Imaging, Physics and Technology, University of Oulu, POB 50, FI-90029 Oulu, Finland.
Email: abdul.kajabi@oulu.fi

## Abstract

Chondral lesions lead to degenerative changes in the surrounding cartilage tissue, increasing the risk of developing post-traumatic osteoarthritis (PTOA). This study aimed to investigate the feasibility of quantitative magnetic resonance imaging (qMRI) for evaluation of articular cartilage in PTOA. Articular explants containing surgically induced and repaired chondral lesions were obtained from the stifle joints of seven Shetland ponies (14 samples). Three age-matched nonoperated ponies served as controls (six samples). The samples were imaged at 9.4 T. The measured qMRI parameters included $T_1$, $T_2$, continuous-wave $T_{1\rho}$ ($CWT_{1\rho}$), adiabatic $T_{1\rho}$ ($AdT_{1\rho}$), and $T_{2\rho}$ ($AdT_{2\rho}$) and relaxation along a fictitious field ($T_{RAFF}$). For reference, cartilage equilibrium and dynamic moduli, proteoglycan content and collagen fiber orientation were determined. Mean values and profiles from full-thickness cartilage regions of interest, at increasing distances from the lesions, were used to compare experimental against control and to correlate qMRI with the references. Significant alterations were detected by qMRI parameters, including prolonged $T_1$, $CWT_{1\rho}$, and $AdT_{1\rho}$ in the regions adjacent to the lesions. The changes were confirmed by the reference methods. $CWT_{1\rho}$ was more strongly associated with the reference measurements and prolonged in the affected regions at lower spin-locking amplitudes. Moderate to strong correlations were found between all qMRI parameters and the reference parameters ($\rho = -0.531$ to $-0.757$). $T_1$, low spin-lock amplitude $CWT_{1\rho}$, and $AdT_{1\rho}$ were most responsive to changes in visually intact cartilage adjacent to the lesions. In the context of PTOA, these findings highlight the potential of $T_1$, $CWT_{1\rho}$, and $AdT_{1\rho}$ in evaluation of compositional and structural changes in cartilage.

**KEYWORDS**

cartilage, osteoarthritis, post-traumatic, quantitative MRI, relaxation times

# 1 | INTRODUCTION

Joint injury is a well-established risk factor in the development of post-traumatic osteoarthritis (PTOA), a chronic disease causing joint pain and dysfunction.[1,2] Injury may be due to fractures, articular cartilage lesions, cruciate or collateral ligament rupture, acute meniscal tear, or a combination of these. Early interventions, like repairing the damaged tissue, or stabilizing the joint, can limit the progression of PTOA.[3] Thus, early detection of articular cartilage damage can constitute an advantage in the prevention and treatment of the respective joint disease.[4]

In addition to direct visualization of articular cartilage, quantitative magnetic resonance imaging (qMRI) provides numerical outcome measures that can be used to nondestructively evaluate early PTOA changes in the tissue.[5,6] MRI relaxation time mapping sequences such as $T_1$, $T_2$, continuous-wave $T_{1\rho}$ (CWT$_{1\rho}$), adiabatic $T_{1\rho}$ (AdT$_{1\rho}$), adiabatic $T_{2\rho}$ (AdT$_{2\rho}$), and relaxation along a fictitious field (T$_{RAFF}$) have been proposed as quantitative biomarkers for the assessment of articular cartilage.[7,8] Native $T_1$ has been linked to interstitial water content of articular cartilage,[9] while $T_2$ has been associated with collagen fiber orientation and tissue hydration.[10,11] CWT$_{1\rho}$ has been linked to changes in proteoglycan (PG) content and collagen network of articular cartilage.[12,13] Moreover, CWT$_{1\rho}$ can be measured at varying spin-locking radio frequency (RF) amplitudes,[14] and has been reported to be selectively sensitive to PG content.[15] Besides repetitive continuous-wave spin-locking method, $T_{1\rho}$ imaging can be performed using adiabatic RF pulses, providing AdT$_{1\rho}$ and AdT$_{2\rho}$,[16] enhancing robustness against field inhomogeneities and reducing sensitivity to magic angle effects.[17] Recent studies of AdT$_{1\rho}$ and AdT$_{2\rho}$ have reported association of the parameters to early OA changes in articular cartilage.[7,18] T$_{RAFF}$ utilizes relaxation during sub-adiabatic RF swept pulses, allowing substantial reduction of specific absorption rate, making it a suitable imaging biomarker in clinical settings.[19]

The aim of this study was to validate the feasibility of $T_1$, $T_2$, CWT$_{1\rho}$, AdT$_{1\rho}$, AdT$_{2\rho}$, and T$_{RAFF}$ relaxation time mapping for evaluation of multiple articular cartilage regions at increasing distances from surgically induced and repaired lesions in an animal model of PTOA. Equine stifle joints were chosen for this study because the cartilage closely resembles that of a human knee.[20] For reference, the qMRI parameters were correlated with equilibrium and dynamic moduli, PG content and collagen fiber orientation. We hypothesize that the qMRI parameters capture the degenerative changes in visually intact cartilage caused by the nearby chondral lesions.

# 2 | METHODS

## 2.1 | Samples

In both stifles of Shetland ponies (N = 7, 6 females, age = 8.8 ± 3.5 years), two 10 mm diameter cartilage lesions were surgically created on the medial femoral ridge to study a cell-containing hydrogel for cartilage repair.[21,22] Each lesion was treated with a combination of chondrons and mesenchymal stem cells (MSCs) in different carrier hydrogels. After 12 months, the animals were sacrificed and triangular wedge-shaped tissue blocks (14 samples), containing both lesions as well as the surrounding tissues, were obtained from the medial femoral ridge (Figure 1). The animal experimentations were carried out at the Surgery division of the Department of Clinical Sciences, Equine Division, Discipline of Orthopaedics and Surgery, Utrecht University, the Netherlands. The procedures were approved by the Ethics Committee of Utrecht University for Animal Experiments in compliance with the Institutional Guidelines on the Use of Laboratory Animals (Permission DEC 2014.III.11.098). As control, similar osteochondral tissue blocks (six samples) were obtained from stifle joints of nonoperated and untreated Shetland ponies (N = 3, age = 10.3 ± 4.7 years) acquired from a local slaughterhouse in the Netherlands.

## 2.2 | Biomechanical measurements

Prior to MRI, all samples (14 experimental and six control) underwent biomechanical indentation testing of cartilage surrounding the repaired lesions, as described before.[21,22] In short, the samples were submerged in phosphate-buffered saline (PBS) and glued on a custom-made sample holder. First, a plane-ended indenter (d = 0.53 mm) was driven in contact with the sample. Then, a stepwise stress-relaxation test (5% strain, ramp velocity of 100%/s and four steps with 10 minute relaxation time after each step), followed by sinusoidal dynamic loading (frequency of 1.0 Hz and strain amplitude of 1%) was conducted to define the equilibrium ($E_{eq}$) and dynamic ($E_{dyn}$) elastic moduli, respectively. The equilibrium and dynamic moduli were calculated in a predefined grid of 12 testing locations in each sample according to the Hayes equation[23] with Poisson's ratios of 0.1 and 0.5, respectively. In this study, a single MRI slice, covering four of the 12 testing locations, was acquired for the analysis (Figure 1E).

## 2.3 | Magnetic resonance imaging

MRI was performed in a 9.4 T vertical bore small animal scanner (Oxford instruments Plc, Witney, UK) using a 19-mm diameter quadrature volume RF transceiver (Rapid Biomedical GmbH, Rimpar, Germany). To provide $^1$H signal-free background, the samples were immersed in perfluoropolyether oil (Galden HS 240, Solvay Solexis, Brussels, Belgium) and placed inside a thin latex container. To minimize the magic angle effect, the samples were positioned in the scanner so as to have the main magnetic field approximately perpendicular to the bone-cartilage interface in the area of interest.

During MRI, a single slice was selected covering the full profile of the cartilage along the four biomechanically tested points ranging distally from the repaired lesion site (Figure 1F). Imaging was conducted with modified magnetization preparation blocks (Table 1) for
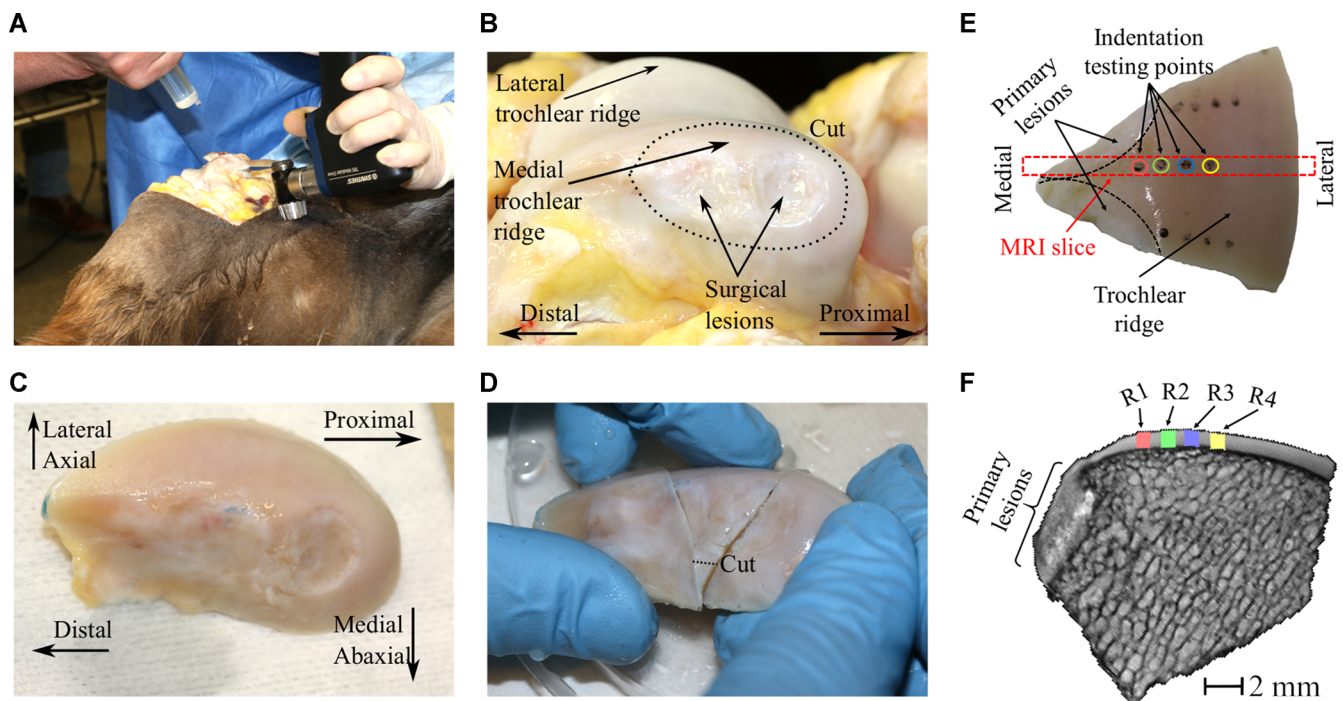
**FIGURE 1** Extraction of the samples. A, Surgeon opened the stifle joint. B, The trochlea was exposed, and the medial ridge was cutoff from the trochlea. C, The medial trochlear ridge. D, Smaller piece from the trochlear osteochondral sample was cutoff to fit it in to the MRI coil. E, Osteochondral sample for MRI. The figure also depicts the biomechanical indentation points and the MRI slice location. F, MR image of the osteochondral sample and the regions of interest that were used in the analyses. MRI, magnetic resonance imaging [Color figure can be viewed at wileyonlinelibrary.com]

$T_1$, $T_2$, $CWT_{1\rho}$,[24] $AdT_{1\rho}$,[16] $AdT_{2\rho}$,[16] and $T_{RAFF}$.[19] The preparation block was coupled with a single-slice fast spin echo (FSE) readout (TR = 5 s [7 s for $T_1$], ETL = 6 [8 for $T_1$ and $CWT_{1\rho}$], $TE_{eff}$ = 4.2 ms, slice thickness = 1 mm, matrix size = 192 × 192, FOV = 19.2 × 19.2 mm$^2$). After collecting the raw MRI data, relaxation time maps (Figure 2) were calculated with Aedes software (http://aedes.uef.fi/) and in-house written plugins using mono-exponential two-parametric fitting on a pixel-by-pixel basis for $T_1$, $T_2$, $CWT_{1\rho}$, $AdT_{1\rho}$, and $AdT_{2\rho}$, and three-parametric mono-exponential fitting with a steady state for $T_{RAFF}$.
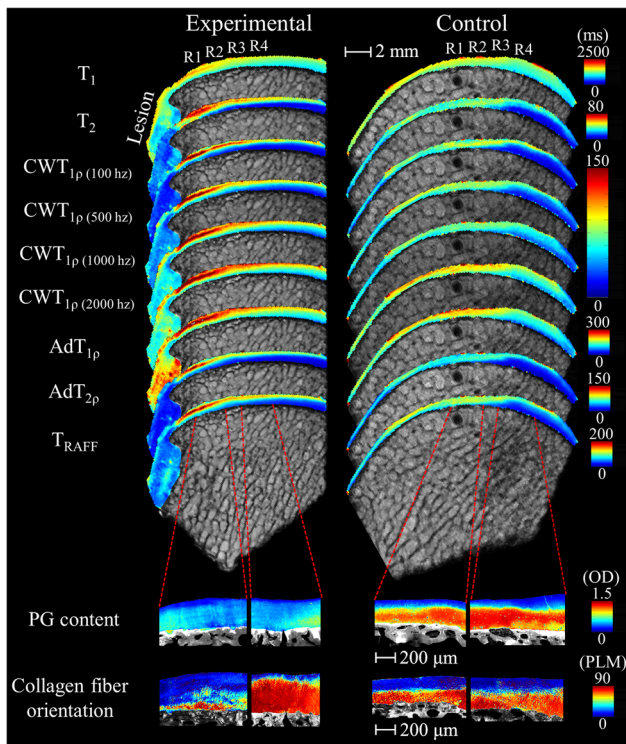
## 2.4 | Digital densitometry and polarized light microscopy

After the MRI, digital densitometry (DD) and polarized light microscopy (PLM) analysis were performed as reported earlier.[25] In brief, the samples were formalin-fixed, decalcified, and sectioned to include the biomechanical testing locations. Optical density (absorbance) of safranin-O was assessed to reveal PG content.[26] In addition, unstained sections digested with hyaluronidase were imaged using PLM to determine collagen fiber orientation.[27]

**TABLE 1** Sequence parameters for MRI protocols

| MRI contrast | Preparation parameters | Pulse power (kHz) | Acquisition time (min:s) |
|---|---|---|---|
| $T_1$ | TI = 200, 500, 800, 1100, 1400, and 3000 ms | | 17:03 |
| $T_2$ | TE = 8.7, 12.6, 18.2, 26.4, 38.2, 55.3, and 80 ms | | 18:82 |
| $CWT_{1\rho}$ | A composite spin-lock embedded between two hard pulses[24] of +90 and −90, TSL = 0, 4, 8, 16, 32, 64, and 128 ms | $\gamma B_1$ = 0.1, 0.2, 0.3, 0.4, 0.5, 0.6, 0.8, 1, and 2 | 110:30 |
| $AdT_{1\rho}$ | Trains of 0, 4, 8, 12, 24, and 36 HS1-AFP pulses,[16] pulse duration 4.5 ms | $\gamma B_{1,max}$ = 2.5 | 16:18 |
| $AdT_{2\rho}$ | Trains of 0, 4, 8, 12, and 24 HS1-AFP pulses between AHP pulses,[16] pulse duration 4.5 ms | $\gamma B_{1,max}$ = 2.5 | 13:50 |
| RAFF | Trains of 0, 2, 4, 8, and 16 RAFF pulses,[19] pulse duration 9 ms | $\gamma B_{1,max}$ = 0.625 | 26:83 |

Abbreviations: AdT1ρ, adiabatic T1ρ; AdT2ρ, adiabatic T2ρ; AFP, adiabatic full-passage; CWT1ρ, continuous-wave T1ρ; RAFF, relaxation along a fictitious field; TI, time to inversion; TE, time to echo; TSL, spin-lock time.

**FIGURE 2** Representative relaxation time maps of $T_1$, $T_2$, continuous-wave (CW) $T_{1\rho}$ at 0.1, 0.5, 1, and 2 kHz, adiabatic $T_{1\rho}$ (Ad$T_{1\rho}$), adiabatic $T_{2\rho}$ (Ad$T_{2\rho}$), and relaxation along a fictitious field ($T_{RAFF}$) for experimental and control samples. Optical density (OD) images, indicative of proteoglycan (PG) content, and collagen orientation (PLM) images represent reference measurements (bottom). Regions R1-R4 indicate the locations of the ROIs and biomechanical testing sites. Increased relaxation times in regions closest to the lesion area were seen in all parameter maps. In line with the prolonged relaxation times, reference images revealed lower PG content and altered collagen fiber orientation in regions closest to the lesion region. PLM, polarized light microscopy; ROIs, regions of interest [Color figure can be viewed at wileyonlinelibrary.com]

## 2.5 | Data analysis

Mean and depth-wise profiles of the relaxation time maps were calculated using four full-thickness cartilage regions of interest (ROIs), which were defined in visually intact cartilage at increasing distances from the repaired lesions and carefully matched with the biomechanical testing points, DD and PLM (Figure 1E,F). The ROIs had the same width but slightly varying depths (due to varying cartilage thickness). The distance of the first region (ROI1) from lesion edge was ~1.6 mm and the distances between the centers of the consecutive ROIs (ROI1-2, ROI2-3, and ROI3-4) were ~3.25 mm. Since the number of pixels along the cartilage depth varied between the samples (ranging from 10 to 20 pixels), all the profiles were normalized along the cartilage thickness. Similarly, depth-wise profiles of the PG content and collagen fiber orientation were obtained from ROIs in the microscope images and normalized along the cartilage thickness. The analysis was performed using a custom-made

algorithm in MATLAB (Matlab R2016b, MathWorks Inc, Natick, MA).

All statistical analyses were performed using SPSS (ver 25, SPSS Inc, IBM Company, Armonk, NY). Normality test (Shapiro-Wilk) confirmed normal distribution of qMRI data but non-normal distribution of the reference data. Thus, differences in qMRI data between experimental and control groups were tested using an independent samples t-test. Regional differences as a function of distance from the repaired lesions were tested using one-way analysis of variance with Tukey post-hoc test. For the non-normally distributed reference data, differences between experimental and control groups were compared using nonparametric two-tailed Mann-Whitney U test, and the regional differences were tested using Kruskal-Wallis test with Dunn-Bonferroni (post-hoc) correction for multiple comparisons. The associations between MRI and reference parameters were studied using Spearman's rank correlation analysis. A P-value of .05 was considered as the limit of statistical significance.

## 2.6 | Data availability

All of the raw data, documentation, and related codes of the study are available for download at the Zenodo archive (http://doi.org/10.5281/zenodo.3893218).

## 3 | RESULTS

### 3.1 | Reference methods

Histological analysis presented larger differences between experimental and control groups in regions closest to the repaired lesions (Figures 2-4). Although differences were nonsignificant, lower PG content and collagen fiber orientation were noted in all regions of the experimental group compared to the corresponding regions in controls (Figures 3 and 4). Comparing the profile plots, collagen fibers in deep cartilage were more aligned with the surface in the regions nearby the lesions in the experimental group, as compared with the corresponding regions in controls, but again these differences were nonsignificant (Figure 3). In general, the farther away from the lesions the smaller the differences between the two groups were.

Overall, significantly lower mean values of dynamic and equilibrium moduli were noted in all regions of the experimental group compared to the corresponding regions in the controls ($P < .05$) (Figure 4). The largest differences were noted in the regions nearby the lesions.

Analyzing regions separately within each group, region 1 (closest to the lesions) had significantly lower equilibrium and dynamic moduli, PG content and collagen fiber orientation compared with regions 3 and 4 in the experimental group ($P < .05$) (Figure 4). In the controls, only equilibrium modulus was significantly lower in region 1 compared to region 4 ($P < .05$) (Figure 4).
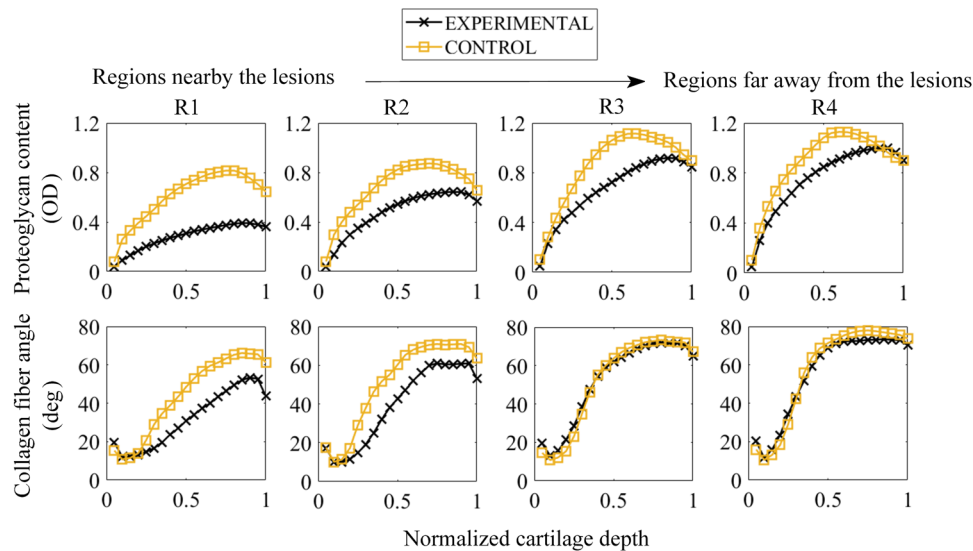
**FIGURE 3**  Mean profiles along cartilage depth (0 = cartilage surface, 1 = bone-cartilage interface) for proteoglycan content and collagen fiber orientation at increasing distances from the lesion area. Region 1 (R1) is closest to the lesion and region 4 (R4) is furthest away from the lesion. Dark yellow lines depict profiles from control samples and black lines from experimental samples [Color figure can be viewed at wileyonlinelibrary.com]

## 3.2 | Magnetic resonance imaging

Overall, visually elevated relaxation time values for all qMRI parameters were observed in the experimental group in regions nearby the lesions, as compared with the regions further away from the lesions on the same sample and in the corresponding regions in the control group (Figures 2, 5-8). $T_1$, $CWT_{1\rho}$, and $AdT_{1\rho}$ had significantly prolonged relaxation time values along the cartilage depth in the experimental group as compared with the control group ($P < .05$) (Figures 5 and 7). The differences between the two groups were most
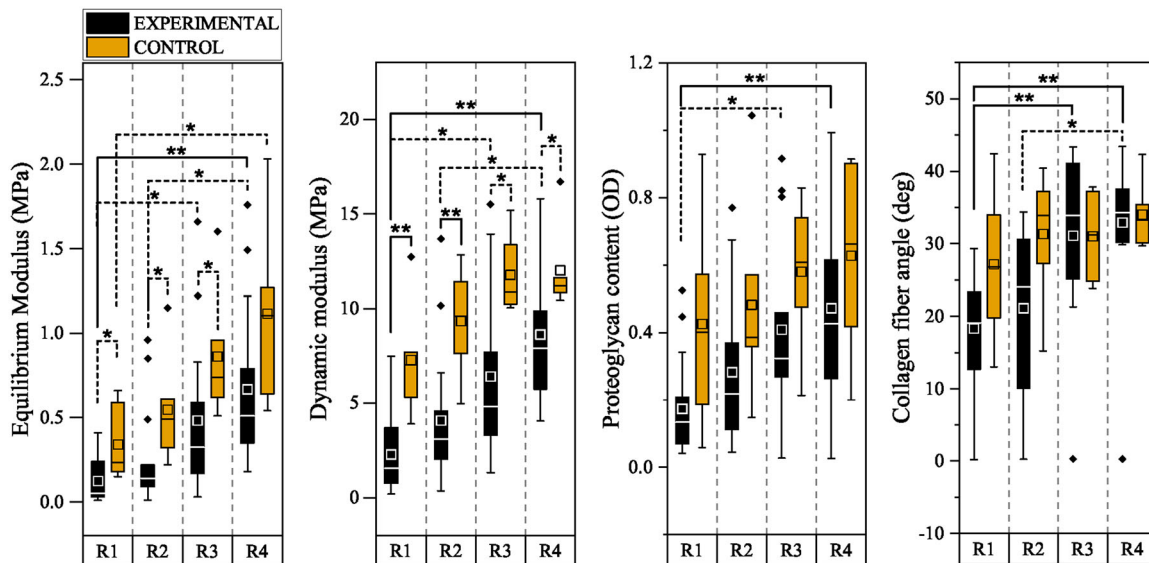


**FIGURE 4**  Boxplots of the biomechanical properties, proteoglycan content and collagen fiber orientation at multiple locations from the lesion area. Region 1 (R1) is closest to the lesion and region 4 (R4) is furthest away from the lesion. Dark yellow bars indicate results from the control and black bars from the experimental samples. The whiskers and the boxes indicate full and 25% to 75% ranges, respectively. Transversal lines and small squares in the boxes represent the median and mean values, respectively. The black solid diamonds are outliers. Pair-wise significant differences are indicated with solid lines (**$P < .01$) and dotted lines (*$P < .05$) [Color figure can be viewed at wileyonlinelibrary.com]
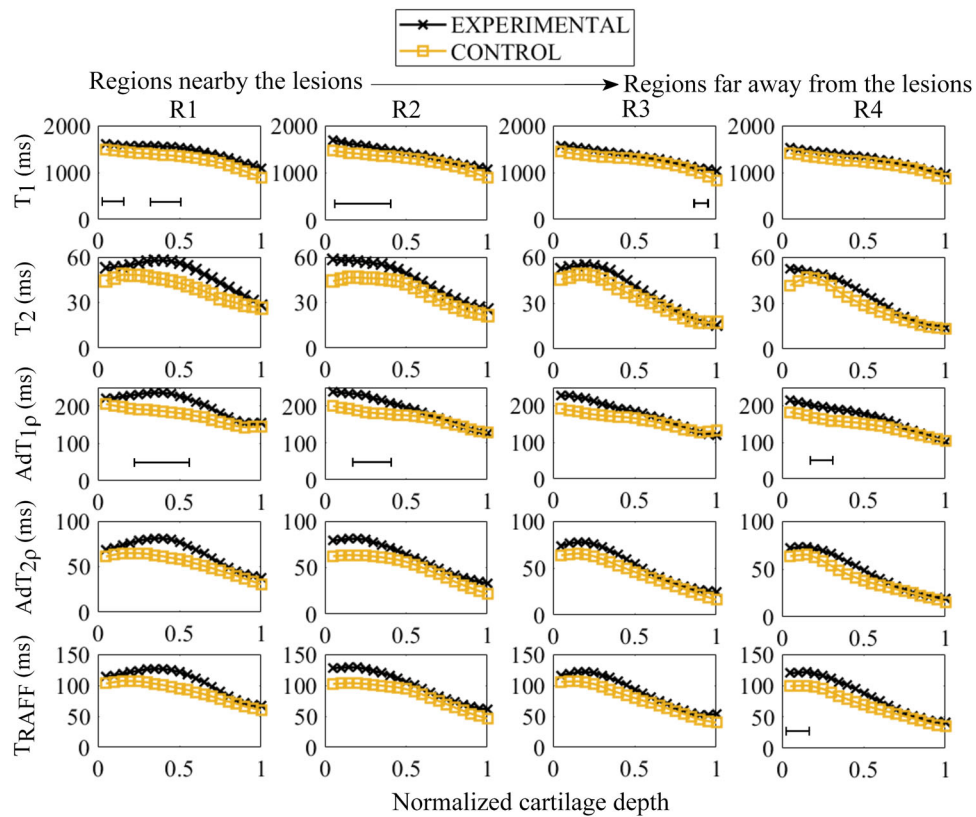
**FIGURE 5** Mean profiles along cartilage depth (0 = cartilage surface, 1 = bone-cartilage interface) for $T_1$, $T_2$, adiabatic $T_{1\rho}$ (AdT$_{1\rho}$), adiabatic $T_{2\rho}$ (AdT$_{2\rho}$), and relaxation along a fictitious field ($T_{RAFF}$) relaxation time at increasing distances from the lesion area. Region 1 (R1) is closest to the lesion and region 4 (R4) is furthest away from the lesion. Dark yellow lines depict profiles from the control and black lines from the experimental samples. Black lines at the bottom of the plots indicate regions where the difference between the control and experimental groups was significant ($P < .05$) [Color figure can be viewed at wileyonlinelibrary.com]
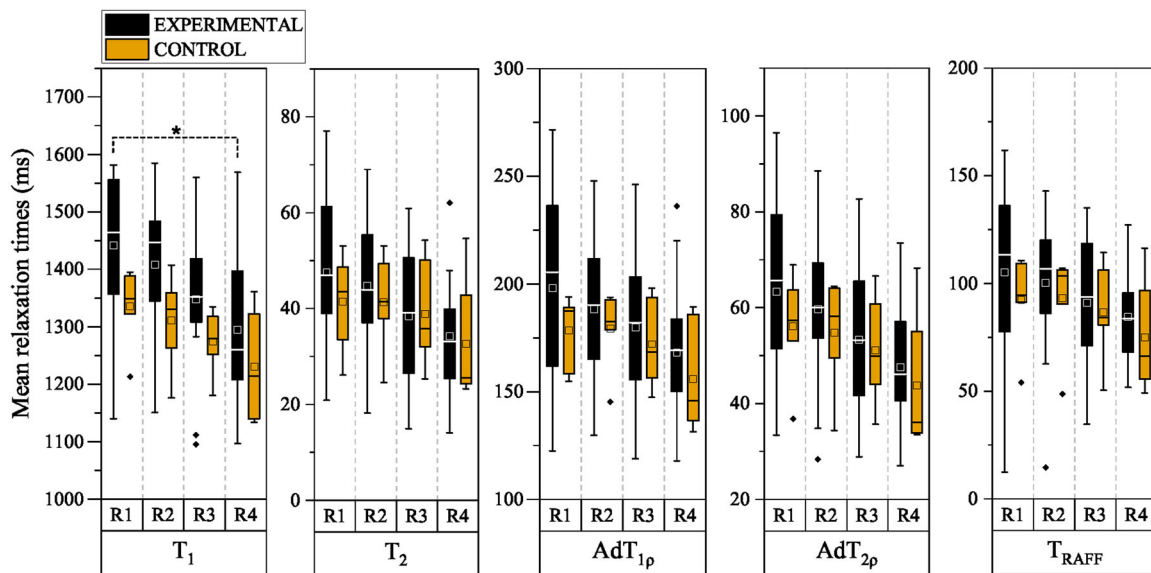


**FIGURE 6** Boxplots of the measured bulk $T_1$, $T_2$, adiabatic $T_{1\rho}$ (AdT$_{1\rho}$), adiabatic $T_{2\rho}$ (AdT$_{2\rho}$), and relaxation along a fictitious field ($T_{RAFF}$) relaxation times at multiple locations from the lesion area. Region 1 (R1) is closest to the lesion and region 4 (R4) is furthest away from the lesion. Dark yellow bars indicate results from the control and black bars from the experimental samples. The whiskers and the boxes indicate full and 25% to 75% ranges, respectively. Transversal lines and small squares in the boxes represent the median and mean values, respectively. The black solid diamonds are outliers. The black solid diamonds are outliers. Pair-wise significant difference is indicated with dotted line (*$P < .05$) [Color figure can be viewed at wileyonlinelibrary.com]
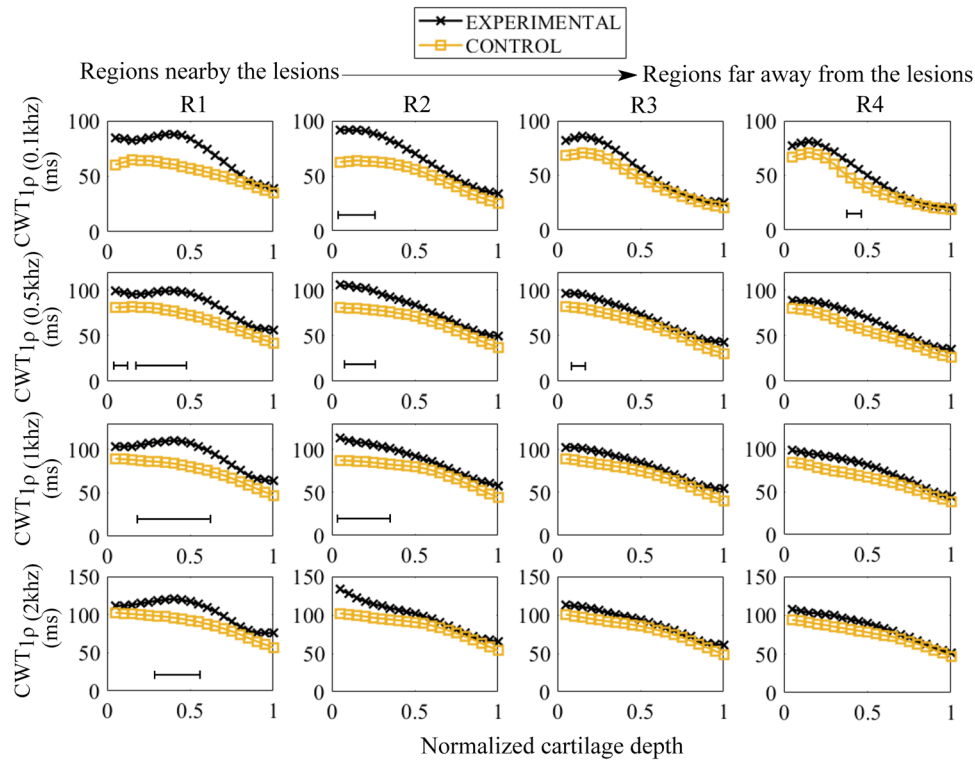
**FIGURE 7** Mean profiles along cartilage depth (0 = cartilage surface and 1 = bone-cartilage interface) for continuous-wave (CW) $T_{1\rho}$ (0.1 Hz), $CWT_{1\rho}$ (0.5 Hz), $CWT_{1\rho}$ (1 kHz), and $CWT_{1\rho}$ (2 kHz) relaxation time at increasing distances from the lesion area. Region 1 (R1) is closest to the lesion and region 4 (R4) is furthest away from the lesion. Dark yellow lines depict profiles from the control and black lines from the experimental samples. Black lines at the bottom of the plots indicate regions where the difference between the control and experimental groups was significant (P < .05) [Color figure can be viewed at wileyonlinelibrary.com]
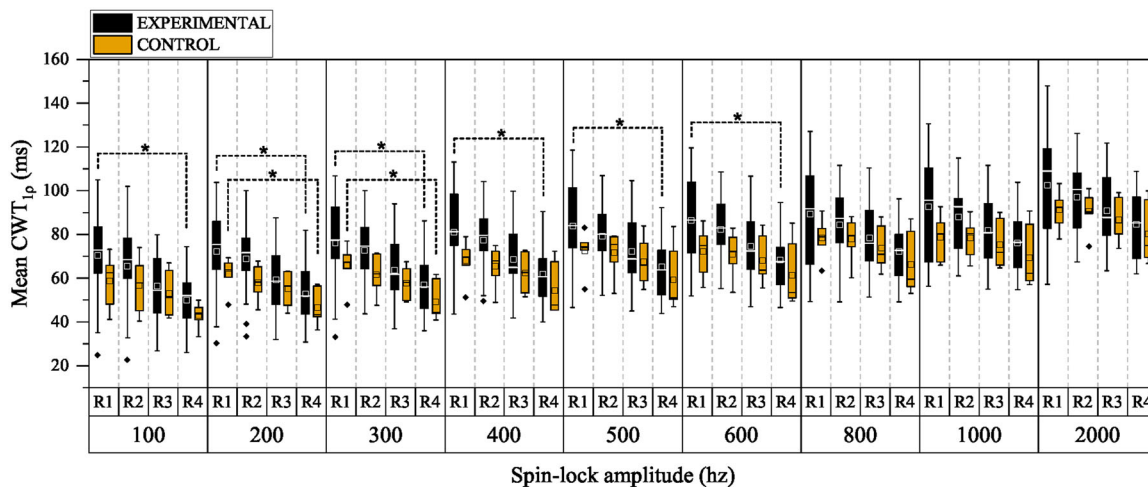


**FIGURE 8** Boxplots of bulk continuous-wave (CW) $T_{1\rho}$ relaxation times measured with increasing spin-locking amplitudes (100–2000 Hz). Region 1 (R1) is closest to the lesion and region 4 (R4) is furthest away from the lesion. Dark yellow bars indicate results from the control and black bars from the experimental samples. The whiskers and the boxes indicate full and 25% to 75% ranges, respectively. Transversal lines and small squares in the boxes represent the median and mean values, respectively. The black solid diamonds are outliers. Pair-wise significant differences are indicated with dotted lines (*P < .05) [Color figure can be viewed at wileyonlinelibrary.com]

**TABLE 2** Spearman's rank correlation coefficients ($r$) between MRI parameters (all data pooled), and equilibrium modulus ($E_{eq}$), dynamic elastic modulus ($E_{dyn}$), optical density (DD, reflective of proteoglycan content), and collagen fiber orientation (PLM)

| MRI parameters | $E_{eq}$ | $E_{dyn}$ | DD | PLM |
| --- | --- | --- | --- | --- |
| $T_1$ | $\rho = -.757^*$ | $\rho = -.708^*$ | $\rho = -.573^*$ | $\rho = -.630^*$ |
| $T_2$ | $\rho = -.602^*$ | $\rho = .531^*$ | $\rho = -.607^*$ | $\rho = -.642^*$ |
| $CWT_{1\rho\ (100\ Hz)}$ | $\rho = -.620^*$ | $\rho = -.559^*$ | $\rho = -.601^*$ | $\rho = -.692^*$ |
| $CWT_{1\rho\ (200\ Hz)}$ | $\rho = -.687^*$ | $\rho = -.629^*$ | $\rho = -.617^*$ | $\rho = -.711^*$ |
| $CWT_{1\rho\ (300\ Hz)}$ | $\rho = -.696^*$ | $\rho = -.645^*$ | $\rho = -.602^*$ | $\rho = -.698^*$ |
| $CWT_{1\rho\ (400\ Hz)}$ | $\rho = -.702^*$ | $\rho = -.662^*$ | $\rho = -.596^*$ | $\rho = -.682^*$ |
| $CWT_{1\rho\ (500\ Hz)}$ | $\rho = -.682^*$ | $\rho = -.627^*$ | $\rho = -.594^*$ | $\rho = -.682^*$ |
| $CWT_{1\rho\ (600\ Hz)}$ | $\rho = -.643^*$ | $\rho = -.623^*$ | $\rho = -.592^*$ | $\rho = -.665^*$ |
| $CWT_{1\rho\ (800\ Hz)}$ | $\rho = -.613^*$ | $\rho = -.572^*$ | $\rho = -.557^*$ | $\rho = -.632^*$ |
| $CWT_{1\rho\ (1000\ Hz)}$ | $\rho = -.595^*$ | $\rho = -.597^*$ | $\rho = -.538^*$ | $\rho = -.602^*$ |
| $CWT_{1\rho\ (2000\ Hz)}$ | $\rho = -.592^*$ | $\rho = -.561^*$ | $\rho = -.534^*$ | $\rho = -.594^*$ |
| $AdT_{1\rho}$ | $\rho = -.608^*$ | $\rho = -.564^*$ | $\rho = -.532^*$ | $\rho = -.563^*$ |
| $AdT_{2\rho}$ | $\rho = -.634^*$ | $\rho = -.559^*$ | $\rho = -.611^*$ | $\rho = -.685^*$ |
| $T_{RAFF}$ | $\rho = -.733^*$ | $\rho = -.678^*$ | $\rho = -.570^*$ | $\rho = -.616^*$ |

Abbreviations: $AdT_{1\rho}$, adiabatic $T_{1\rho}$; $AdT_{2\rho}$, adiabatic $T_{2\rho}$; $CWT_{1\rho}$, continuous-wave $T_{1\rho}$; RAFF, relaxation along a fictitious field.
$^*P < .001$.

pronounced in the upper half of the cartilage depth and in the regions nearest to the lesions (Figures 5 and 7). For $CWT_{1\rho}$, the differences between the experimental and control groups were mostly noted at spin-lock amplitudes of 0.2 to 1 kHz (Figure 7). When comparing the mean values, no significant differences between the two groups were detected in their respective regions (Figures 6 and 8).

In the regional analysis, all qMRI parameters had wider ranges across the regions in the experimental group compared with the regions in the controls (Figures 6 and 8). $T_1$ and $CWT_{1\rho}$ were significantly prolonged in region 1 (closest to the lesions) compared with region 4 (furthest away from the lesions) ($P < .05$) (Figures 6 and 8). In the experimental group, the regional difference was significant for $T_1$ and $CWT_{1\rho}$ at spin-lock amplitudes (100-600 Hz), and in case of the control group, the difference was significant with $CWT_{1\rho}$ at spin-lock amplitudes ($P < .05$) (200-300 Hz).

## 3.3 | Correlation analysis

For pooled data (experimental and control groups together), all the correlation coefficients between the qMRI and reference parameters were statistically significant and ranged from −0.531 to −0.757 (Table 2). The highest correlation was found between $T_1$ and equilibrium modulus ($\rho = -0.757$). Moreover, $T_{RAFF}$, $T_1$, and $CWT_{1\rho}$ at spin-locking amplitude (200 Hz) were strongly correlated with the equilibrium modulus, dynamic modulus, and collagen fiber orientation,

respectively (Table 2). In general, $CWT_{1\rho}$ had stronger correlations with the reference parameters towards the lower spin-locking amplitudes (200-600 Hz) (Table 2).

## 4 | DISCUSSION

This study investigated the potential of qMRI relaxation time mapping for the assessment of the development of PTOA induced by surgically created-and-repaired chondral lesions in the stifle of ponies. The most important finding was that qMRI relaxation properties of cartilage were altered due to PTOA and were dependent on the distance from the lesions. The changes were coincident with those found with the reference methods, which included an increase in biomechanical moduli and PG content and changes in the collagen fiber network architecture towards typical healthy cartilage as a function of increasing distance from the lesions. Moreover, the analysis revealed moderate to strong correlations between the qMRI and reference parameters.

As reported previously in separate studies of the same specimens,[22,25] biomechanical indentation testing as well as quantitative microscopy (DD and PLM) revealed degenerative changes in regions nearby the chondral lesions. Quantitative microscopy showed large variations in the depth-wise profiles between the experimental and control groups in the regions closest to the chondral lesions, while the depth-wise profiles of the two groups almost overlapped one another in the regions further away from the lesions. Previous studies using the equine chondral lesion model have also reported alterations in the composition and biomechanical properties of articular cartilage.[28,29]

In this study, multiple qMRI parameters, including $T_1$, $T_2$, $CWT_{1\rho}$, $AdT_{1\rho}$, $AdT_{2\rho}$, and $T_{RAFF}$, were used to study degenerative changes in articular cartilage due to presence of adjacent lesions. The depth-wise profiles of qMRI parameters revealed the changes between the two groups in the upper half of the cartilage depth and in regions adjacent to the lesions and followed the same trend as quantitative histology. It is known that degenerative OA changes in articular cartilage are progressive and commonly initiate from the superficial zone.[30-32] The results of this study suggest that degeneration in PTOA propagates from the lesions to the adjacent tissues starting from the superficial zones. These findings suggest the potential of qMRI parameters in tracking the progression of PTOA from a cartilage lesion towards the surrounding cartilage tissue.

The number of studies on $T_1$ relaxation time constant without contrast agent is very limited.[9,10,33,34] In the present study, $T_1$ along with $CWT_{1\rho}$ and $AdT_{1\rho}$ were the only qMRI parameters to differentiate affected regions adjacent to the chondral lesions from least affected regions further away from the lesions. Previous studies of $T_1$ have also reported the sensitivity of the parameter to degenerative changes in cartilage.[34,35] Moreover, $T_1$ had the strongest correlation with the biomechanical modulus of cartilage, which is consistent with previous studies.[33,36] $T_1$ relaxation is most effective when the time component of the local field fluctuations matches the resonant

frequency of the water protons. High concentration of macro-molecules in healthy cartilage increases the probability of the macromolecular interactions with water protons, shortening $T_1$ relaxation due to effective energy transfer between the spins and the lattice. In case of degenerated cartilage, depleted extracellular matrix induces an increase in the tissue hydration, which can lead to reduced mechanical stiffness as well as result in prolonged $T_1$.[9,33,36] These findings suggest that $T_1$ is sensitive to the degenerative alterations in articular cartilage and may deserve more attention in the evaluation of cartilage than it has received so far.

$T_2$ is generally considered to be sensitive to changes of the collagen fiber network of articular cartilage.[10,37,38] In the present study, $T_2$ could visually reveal differences in affected regions nearby the lesions from similar regions in controls, although changes were nonsignificant. Moreover, the relaxation time parameter was moderately correlated with biomechanical stiffness, PG content and the collagen fiber orientation angle. Similarly, Hirose et al[39] reported no significant change in $T_2$ values with cartilage degeneration compared to healthy cartilage. However, numerous studies have used $T_2$ in clinical studies demonstrating its ability to reveal cartilage degeneration.[40,41]

$CWT_{1\rho}$ at different spin-locking amplitudes demonstrated variable responses to tissue changes induced by the chondral lesions. Towards the lower spin-lock amplitudes (0.2-1 kHz), $CWT_{1\rho}$ was able to discriminate tissue alterations in regions nearby the lesions from regions further away from the lesions. This could be due to large contribution of dipolar interactions and chemical exchange to the relaxation time at lower spin-lock amplitudes.[15,42] On the other hand, moderate to strong correlation was found between all the applied spin-lock amplitudes and the reference methods. The quantitative microscopy results were of particular interest, showing an increasing association of PG content and collagen fiber orientation with $CWT_{1\rho}$ towards the lower spin-lock amplitudes, which is consistent with the findings of a previous ex vivo human study.[13] Thus, current results on low spin-locking amplitude $CWT_{1\rho}$ indicate that the parameter is more correlated with collagen orientation than with the PG content. Furthermore, the correlation of $CWT_{1\rho}$ with the collagen orientation is comparable with that of $T_2$. However, numerous studies have primarily demonstrated the relation between $CWT_{1\rho}$ and PG content[12,13,15,42]; although the association of the relaxation parameter with the collagen network have also been reported.[13,43] The findings of the present study suggest that $CWT_{1\rho}$ at lower spin-lock amplitudes ($\gamma B_1 \leq 1$ kHz) are more sensitive to the degenerative changes in cartilage compared with the higher amplitudes ($\gamma B_1 > 1$ kHz), which supports the use of $CWT_{1\rho}$ imaging in the clinical setting, where higher spin-locking amplitudes may not be achievable.

In contrast to $CWT_{1\rho}$, where constant spin-lock amplitude RF is applied, in $AdT_{1\rho}$, $AdT_{2\rho}$, and $T_{RAFF}$ the spin-lock amplitude is modulated over time, creating a wide range of effective frequencies and extending the sensitivity of these parameters to molecular fluctuations.[44-46] Previous studies of $AdT_{1\rho}$, $AdT_{2\rho}$, and $T_{RAFF}$ have demonstrated the high sensitivity of the MRI parameters to cartilage degeneration.[7,13,47,48] Recent clinical studies of $AdT_{1\rho}$ and $AdT_{2\rho}$

reported the association of these parameters with cartilage loss, clinical OA features and meniscal tear.[48,49] In the current study, $AdT_{1\rho}$ was one of the three parameters, besides $T_1$ and $CWT_{1\rho}$, to reveal PTOA changes in multiple locations adjacent to the lesions. Examining the correlation analyses, $T_{RAFF}$ was strongly associated to equilibrium modulus, with $AdT_{1\rho}$ and $AdT_{2\rho}$ showing moderate correlations with the reference parameters.

Though the experimental setup and the sequence parameters were optimized for the qMRI, certain limitations were identified in this study. The sample size for the control group was relatively small (six samples), which reduces the statistical power and resulted in asymmetric comparison with the experimental group (14 samples). The relatively small sample size of the control group did not significantly impair this study, however, as the goal was to investigate the feasibility of the qMRI methods in detecting chronic changes due to lesions in the experimental group. The size of the lesion has been reported to be critical in the disease progression.[50] In this study, the lesions were of approximately the same size, limiting the assessment and discussion of the effect of the lesion size on the extension of the degeneration in the surrounding cartilage tissue. In addition, the data points from biomechanical indentation and histology were not coregistered with the qMRI ROIs. However, visual markers (Figure 1E,F) were used to indicate the locations of the biomechanical indentation testing, which were then carefully and consistently followed through in histology and qMRI measurements and analysis. Finally, the conclusions drawn in this ex vivo study were based on high resolution images acquired at 9.4 T. Further in vivo clinical studies are needed to prove the technical translatability and clinical utility of the qMRI parameters. In particular, $T_1$ relaxation is field dependent and measurements at varying field strengths may probe different properties of cartilage tissue.

In conclusion, this study reports the potential of multiple qMRI relaxation parameters in noninvasive monitoring the progression of PTOA in the cartilage surrounding surgically induced lesions. $T_1$, low spin-lock amplitude $CWT_{1\rho}$ and $AdT_{1\rho}$ were most responsive to the degenerative changes, corresponding with biomechanical stiffness and histological measurements of the cartilage tissue. Moreover, $T_1$ had the strongest association with the biomechanical properties of the cartilage tissue, which deserves more attention in clinical studies of articular cartilage. $CWT_{1\rho}$ was more sensitive to the degenerative changes towards the lower spin-lock amplitudes. $T_2$ values did not significantly change in the affected regions and were less correlated to collagen orientation compared with $CWT_{1\rho}$. In the context of PTOA, these findings highlight the potential of $T_1$, $CWT_{1\rho}$ at clinically feasible spin-lock amplitudes and $AdT_{1\rho}$, for the evaluation of structural changes of articular cartilage.

## ACKNOWLEDGMENTS

## CONFLICT OF INTERESTS

All the authors declare that there are no conflict of interests.

## AUTHOR CONTRIBUTIONS

AWK: qMRI map calculation, PLM measurement, data analysis, and manuscript drafting. VC: interpretation of results and supervising, and manuscript editing. JKS: sample preparation, indentation testing, OD measurements, and manuscript editing. JHK: MRI measurements, MRI ROI definitions, and manuscript editing. ON: PLM measurement and manuscript editing. NCRteM: animal experiments, indentation testing, and manuscript editing. IADM, JV, HB, PRvanW, and JM: animal experiments, design of the study, and manuscript editing. JT: design of the study and manuscript editing. MTN: design of the study, interpretation of results and supervising, and manuscript editing. MJN: design of the study, MRI measurements, interpretation of results and supervising, and manuscript drafting and editing. All authors: revision for intellectual content and final approval.

## ORCID

*Abdul Wahed Kajabi* http://orcid.org/0000-0001-7670-8134

*Victor Casula* https://orcid.org/0000-0003-0447-2796

*Olli Nykänen* http://orcid.org/0000-0001-7329-3463

*Mikko J. Nissi* http://orcid.org/0000-0002-5678-0689

## REFERENCES

1. Thomas AC, Hubbard-Turner T, Wikstrom EA, Palmieri-Smith RM. Epidemiology of posttraumatic osteoarthritis. *J Athl Train*. 2017;52: 491-496.
2. Buckwalter JA, Brown TD. Joint injury, repair, and remodeling: Roles in post-traumatic osteoarthritis. *Clin Orthop Relat Res*. 2004;423:7-16.
3. Anderson DD, Chubinskaya S, Guilak F, et al. Post-traumatic osteoarthritis: improved understanding and opportunities for early intervention. *J Orthop Res*. 2011;29:802-809.
4. Bolcos PO, Mononen ME, Tanaka MS, et al. Identification of locations susceptible to osteoarthritis in patients with anterior cruciate ligament reconstruction: combining knee joint computational modelling with follow-up T1$\rho$ and T2 imaging. *Clin Biomech*. 2019:104844.
5. Oei EH, van Tiel J, Robinson WH, Gold GE. Quantitative radiologic imaging techniques for articular cartilage composition: toward early diagnosis and development of disease-modifying therapeutics for osteoarthritis. *Arthritis Care Res*. 2014;66:1129-1141.
6. Nieminen MT, Casula V, Nevalainen MT, Saarakkala SS. Osteoarthritis year in review 2018: Imaging. *Osteoarthr Cartil*. 2018;27:401-411.
7. Rautiainen J, Nissi MJ, Liimatainen T, Herzog W, Korhonen RK, Nieminen MT. Adiabatic rotating frame relaxation of MRI reveals early cartilage degeneration in a rabbit model of anterior cruciate ligament transection. *Osteoarthr Cartil*. 2014;22:1444-1452.
8. Nebelung S, Post M, Knobe M, et al. Detection of early-stage degeneration in human articular cartilage by multiparametric MR imaging mapping of tissue functionality. *Sci Rep*. 2019;9:5895.
9. Berberat JE, Nissi MJ, Jurvelin JS, Nieminen MT. Assessment of interstitial water content of articular cartilage with T1 relaxation. *Magn Reson Imag*. 2009;27:727-732.
10. Xia Y. Relaxation anisotropy in cartilage by NMR microscopy ($\mu$MRI) at 14-$\mu$m resolution. *Magn Reson Med*. 1998;39:941-949.
11. Nieminen MT, Rieppo J, Töyräs J, et al. T2 relaxation reveals spatial collagen architecture in articular cartilage: a comparative quantitative MRI and polarized light microscopic study. *Magn Reson Med*. 2001;46: 487-493.
12. Akella SV, Regatte RR, Gougoutas AJ, et al. Proteoglycan-induced changes in T1$\rho$-relaxation of articular cartilage at 4T. *Magn Reson Med*. 2001;46:419-423.
13. Rautiainen J, Nissi MJ, Salo EN, et al. Multiparametric MRI assessment of human articular cartilage degeneration: correlation with quantitative histology and mechanical properties. *Magn Reson Med*. 2015;74:249-259.
14. Sepponen RE, Pohjonen JA, Sipponen JT, Tanttu JI. A method for T1 rho imaging. *J Comput Assist Tomogr*. 1985;9:1007-1011.
15. Duvvuri U, Reddy R, Patel SD, Kaufman JH, Kneeland JB, Leigh JS. T1?-relaxation in articular cartilage: effects of enzymatic degradation. *Magn Reson Med*. 1997;38:863-867.
16. Michaeli S, Sorce DJ, Garwood M. T2$\rho$ and T1$\rho$ adiabatic relaxations and contrasts. *Curr Anal Chem*. 2008;4:8-25.
17. Hanninen N, Rautiainen J, Rieppo L, Saarakkala S, Nissi MJ. Orientation anisotropy of quantitative MRI relaxation parameters in ordered tissue. *Sci Rep*. 2017;7:9606-017-10053-2.
18. Casula V, Nissi MJ, Podlipská J, et al. Elevated adiabatic T1$\rho$ and T2$\rho$ in articular cartilage are associated with cartilage and bone lesions in early osteoarthritis: a preliminary study. *J Magn Reson Imag*. 2017;46: 678-689.
19. Liimatainen T, Sorce DJ, O'connell R, Garwood M, Michaeli S. MRI contrast from relaxation along a fictitious field (RAFF). *Magn Reson Med*. 2010;64:983-994.
20. McIlwraith CW, Fortier LA, Frisbie DD, Nixon AJ. Equine models of articular cartilage repair. *Cartilage*. 2011;2:317-326.
21. Sarin JK, Te Moller N, Mancini I, et al. Arthroscopic near infrared spectroscopy enables simultaneous quantitative evaluation of articular cartilage and subchondral bone in vivo. *Sci Rep*. 2018;8:13409.
22. Nykänen O, Sarin JK, Ketola JH, et al. T2* and quantitative susceptibility mapping in an equine model of post-traumatic osteoarthritis: assessment of mechanical and structural properties of articular cartilage. *Osteoarthr Cartil*. 2019;27:1481-1490.
23. Hayes W, Keer L, Herrmann G, Mockros L. A mathematical analysis for indentation tests of articular cartilage. *J Biomech*. 1972;5:541-551.
24. Witschey WR, Borthakur A, Elliott MA, et al. Artifacts in T1$\rho$-weighted imaging: compensation for B 1 and B 0 field imperfections. *J Magn Reson*. 2007;186:75-85.
25. Sarin JK, Nykänen O, Tiitu V, et al. Arthroscopic determination of cartilage proteoglycan content and collagen network structure with near-infrared spectroscopy. *Ann Biomed Eng*. 2019;47:1-12.
26. Kiviranta I, Jurvelin J, Säämänen A, Helminen H. Microspectrophotometric quantitation of glycosaminoglycans in articular cartilage sections stained with safranin O. *Histochemistry*. 1985;82:249-255.
27. Rieppo J, Hallikainen J, Jurvelin JS, Kiviranta I, Helminen HJ, Hyttinen MM. Practical considerations in the use of polarized light microscopy in the analysis of the collagen network in articular cartilage. *Microsc Res Tech*. 2008;71:279-287.
28. Strauss EJ, Goodrich LR, Chen C, Hidaka C, Nixon AJ. Biochemical and biomechanical properties of lesion and adjacent articular cartilage after chondral defect repair in an equine model. *Am J Sports Med*. 2005;33:1647-1653.
29. Alwan W, Carter S, Bennett D, Edwards G. Glycosaminoglycans in horses with osteoarthritis. *Equine Vet J*. 1991;23:44-47.
30. Korhonen RK, Wong M, Arokoski J, et al. Importance of the superficial tissue layer for the indentation stiffness of articular cartilage. *Med Eng Phys*. 2002;24:99-108.
31. Buckwalter JA, Mankin H. Instructional course lectures, the american academy of orthopaedic surgeons-articular cartilage. part II: degeneration and osteoarthrosis, repair, regeneration, and transplantation. *J Bone Jt Surg*. 1997;79:612-632.
32. Kajabi AW, Casula V, Ojanen S, et al. Multiparametric MR imaging reveals early cartilage degeneration at 2 and 8 weeks after ACL transection in a rabbit model [published online ahead of print March 04, 2020]. *J Orthop Res*. https://doi.org/10.1002/jor.24644

33. Nissi MJ, Salo EN, Tiitu V, et al. Multi-parametric MRI characterization of enzymatically degraded articular cartilage. *J Orthop Res.* 2016; 34:1111-1120.

34. Xia Y, Wang N, Lee J, Badar F. Strain-dependent T1 relaxation profiles in articular cartilage by MRI at microscopic resolutions. *Magn Reson Med.* 2011;65:1733-1737.

35. Lin P, Reiter DA, Spencer RG. Classification of degraded cartilage through multiparametric MRI analysis. *J Magn Reson.* 2009;201: 61-71.

36. Wayne JS, Kraft KA, Shields KJ, Yin C, Owen JR, Disler DG. MR imaging of normal and matrix-depleted cartilage: Correlation with biomechanical function and biochemical composition. *Radiology.* 2003; 228:493-499.

37. Xia Y, Moody JB, Alhadlaq H. Orientational dependence of T2 relaxation in articular cartilage: a microscopic MRI (μMRI) study. *Magn Reson Med.* 2002;48:460-469.

38. Nissi MJ, Rieppo J, Töyräs J, et al. T2 relaxation time mapping reveals age-and species-related diversity of collagen network architecture in articular cartilage. *Osteoarthr Cartil.* 2006;14: 1265-1271.

39. Hirose J, Nishioka H, Nakamura E, Oniki Y, Yamashita Y, Mizuta H. T1ρ and T2 mapping of the proximal tibiofibular joint in relation to aging and cartilage degeneration. *Eur J Radiol.* 2012;81: 2776-2782.

40. Dunn TC, Lu Y, Jin H, Ries MD, Majumdar S. T2 relaxation time of cartilage at MR imaging: comparison with severity of knee osteoarthritis. *Radiology.* 2004;232:592-598.

41. Baum T, Joseph GB, Arulanandan A, et al. Association of magnetic resonance imaging–based knee cartilage T2 measurements and focal knee lesions with knee pain: data from the osteoarthritis initiative. *Arthritis Care Res.* 2012;64:248-255.

42. Akella SV, Regatte RR, Wheaton AJ, Borthakur A, Reddy R. Reduction of residual dipolar interaction in cartilage by spin-lock technique. *Magn Reson Med.* 2004;52:1103-1109.

43. Mlynarik V, Szomolanyi P, Toffanin R, Vittur F, Trattnig S. Transverse relaxation mechanisms in articular cartilage. *J Magn Reson.* 2004;169: 300-307.

44. Mangia S, Liimatainen T, Garwood M, Michaeli S. Rotating frame relaxation during adiabatic pulses vs. conventional spin lock: Simulations and experimental results at 4 T. *Magn Reson Imag.* 2009;27: 1074-1087.

45. Garwood M, DelaBarre L. The return of the frequency sweep: designing adiabatic pulses for contemporary NMR. *J Magn Reson.* 2001; 153:155-177.

46. Liimatainen T, Sorce DJ, O'connell R, Garwood M, Michaeli S. MRI contrast from relaxation along a fictitious field (RAFF). *Magn Reson Med.* 2010;64:983-994.

47. Ellermann J, Ling W, Nissi MJ, et al. MRI rotating frame relaxation measurements for articular cartilage assessment. *Magn Reson Imaging.* 2013;31:1537-1543.

48. Casula V, Nissi MJ, Podlipská J, et al. Elevated adiabatic T1ρ and T2ρ in articular cartilage are associated with cartilage and bone lesions in early osteoarthritis: a preliminary study. *J Magn Reson Imag.* 2017;46: 678-689.

49. Kajabi AW, Casula V, Nissi MJ, et al. Assessment of meniscus with adiabatic T1ρ and T2ρ relaxation time in asymptomatic subjects and patients with mild osteoarthritis: a feasibility study. *Osteoarthr Cartil.* 2018;26:580-587.

50. Salonius E, Rieppo L, Nissi MJ, et al. Critical-sized cartilage defects in the equine carpus. *Connect Tissue Res.* 2019;60:95-106.